The 8th European Congress on Computational Methods in Applied Sciences and Engineering
ECCOMAS Congress 2022
5-9 June 2022, Oslo, Norway

ON THE EFFECT OF PRANDTL NUMBER TO SUBGRID-SCALE HEAT FLUX MODELS

F.X. Trias[1], D. Santos[1], J.A. Hopman[1], A. Gorobets[2], A. Oliva[1]

[1] Heat and Mass Transfer Technological Center, Technical University of Catalonia
C/Colom 11, 08222 Terrassa (Barcelona)
{francesc.xavier.trias,daniel.santos.serrano,jannes.hopman,asensio.oliva}@upc.edu

[2] Keldysh Institute of Applied Mathematics, 4A, Miusskaya Sq., Moscow 125047, Russia
andrey.gorobets@gmail.com

Key words: LES, SGS models, buoyancy-driven turbulence, Rayleigh-Bénard convection, Prandtl number effect, ultimate regime

Abstract. Estimations of the grid size and computational cost for direct numerical simulation (DNS) and large-eddy simulation (LES) of Rayleigh-Bénard convection (RBC) are presented in the $\{Ra, Pr\}$ phase space. Computational requirements to reach the so-called asymptotic Kraichnan or ultimate regime of turbulence using DNS are far too expensive. Therefore, we turn to LES to predict the large-scale behavior at very high Ra-numbers. However, *a priori* alignment studies clearly show why the modelization of the SGS heat flux is the main difficulty that (still) precludes reliable LES of buoyancy-driven flows at (very) high Ra-numbers. This inherent difficulty can be by-passed by carrying out simulations at low-Pr numbers where no SGS heat flux activity is expected. This opens the possibility to reach the ultimate regime carrying out LES of RBC at low-Pr using meshes of $10^{10} - 10^{11}$ grid points. Nevertheless, to do so, we firstly need to combine proper numerical techniques for LES (also DNS) with an efficient use of modern hybrid supercomputers.

1 INTRODUCTION

Buoyancy-driven flows have always been an important subject of scientific studies with numerous applications in environment and technology. The most famous example thereof is the thermally driven flow developed in a fluid layer heated from below and cooled from above, *i.e.* the Rayleigh-Bénard convection (RBC). It constitutes a canonical flow configuration that resembles many natural and industrial processes, such as solar thermal power plants, indoor space heating and cooling, flows in nuclear reactors, electronic devices, and convection in the atmosphere, oceans and the deep mantle.

In the last decades significant efforts, both numerically and experimentally, have been directed at investigating the mechanisms and the detailed scaling behavior of the Nusselt (Nu) number as a function of Rayleigh (Ra) and Prandtl (Pr) numbers in the general form $Nu \propto Ra^{\gamma} Pr^{\beta}$. In this

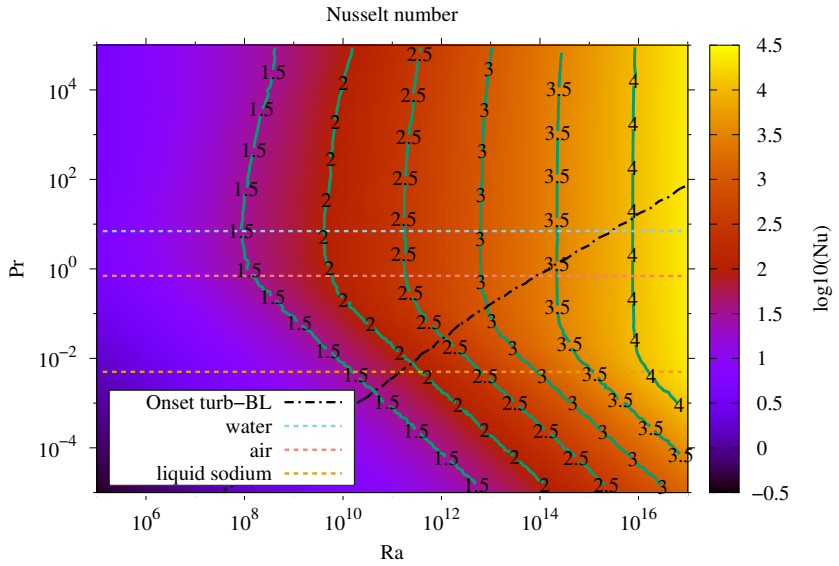

Figure 1: Estimation of the Nusselt number of a RBC in the $\{Ra, Pr\}$ phase space given by the classical GL theory [1] and its subsequent corrections [2]. Green solid isolines represent the $log10$ of the Nusselt. Three dashed horizontal lines correspond to three different working fluids: water ($Pr = 7$), air ($Pr = 0.7$) and liquid sodium ($Pr = 0.005$). Black dash-dotted line is an estimation for the onset of turbulence in the thermal boundary layer.

regard, Figure 1 shows the predictions of the Nu-number based on the classical Grossmann-Lohse (GL) theory [1] and its subsequent corrections [2, 3] where different scaling regimes, characterized by their corresponding exponents γ and β, are identified. Assuming this power-law scalings and following the same reasonings as in Ref. [4] leads to the estimations for the number of grid points shown in Figure 2 (top). This corresponds to mesh resolution requirements for DNS and clearly explain why nowadays DNS of RBC is still limited to relatively low Ra-numbers. However, many of the above-mentioned applications are governed by much higher Ra numbers, located in the region of the $\{Ra, Pr\}$ phase space where the thermal boundary layer becomes turbulent (see the black dash-dotted line in Figure 2). This region corresponds to the so-called asymptotic Kraichnan or ultimate regime of turbulence, with $\gamma = 1/2$. On the other hand, reaching such Ra-numbers experimentally while keeping the basic assumptions (Boussinesq approximation, adibaticity of the closing walls, isothermal horizontal walls, perfectly smooth surfaces...) is a very hard task; therefore, the observation of the Kraichnan regime also remains elusive [2, 3].

2 LARGE-EDDY SIMULATION OF BUOYANCY-DRIVEN TURBULENCE: CHALLENGES AND OPPORTUNITIES

2.1 Antecedents and failure of the eddy-diffusivity models

In this context, we may turn to LES to predict the large-scale behavior of incompressible turbulent flows driven by buoyancy at very high Ra-numbers. In LES, the large-scale motions are explicitly computed, whereas the effects of small-scale motions are modeled. Since the ad-

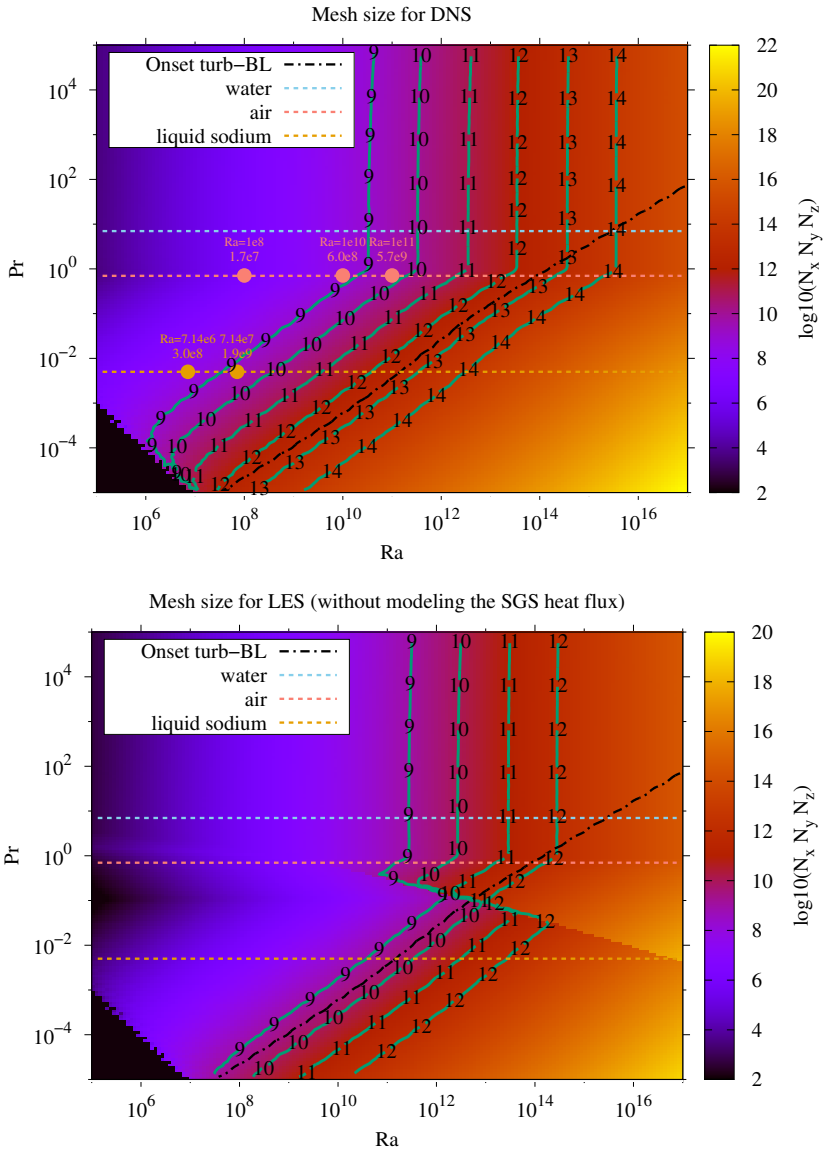

Figure 2: Estimation of the mesh sizes for DNS (top) and LES (bottom) simulations of RBC in the $\{Ra, Pr\}$ phase space. LES estimations assume that thermal scales are fully resolved, *i.e.* no SGS heat flux model is needed. Green solid isolines represent the $log10$ of the total number of grid points. Three dashed horizontal lines correspond to three different working fluids: water ($Pr = 7$), air ($Pr = 0.7$) and liquid sodium ($Pr = 0.005$). Dots displayed on top of these lines correspond to the DNS simulations carried out in previous studies [4–6]. Black dash-dotted line is an estimation for the onset of turbulence in the thermal boundary layer.

vent of CFD, many subgrid-scale (SGS) models have been proposed and successfully applied to a wide range of flows. However, there still exits inherent difficulties in the proper modelization of the SGS heat flux. This was analyzed in detail in the PRACE project entitled "Exploring

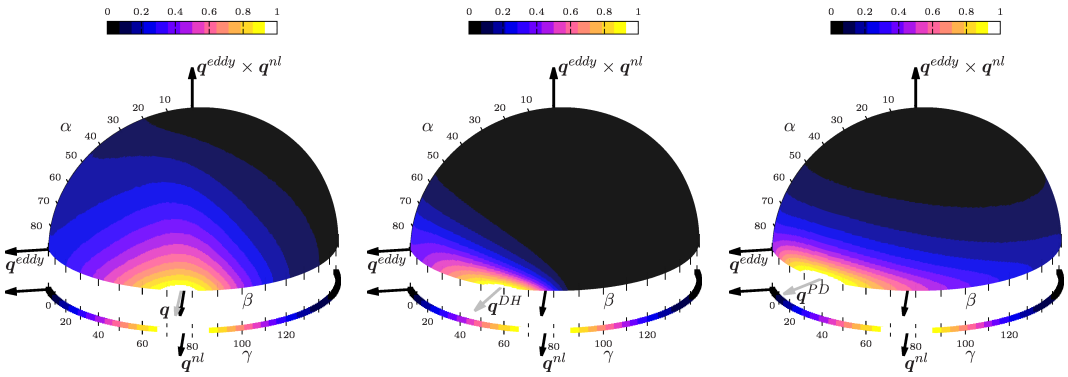

Figure 3: Joint probability distribution functions (PDF) of the angles (α, β) plotted on a half unit sphere to show the orientation in the space of the mixed model. From left to right, alignment trends of the actual SGS heat flux, $\boldsymbol{q}$, the Daly and Harlow [7] model (Eq. 6) and the Peng and Davidson [8] model (Eq. 5). For simplicity, the JPDF and the PDF magnitudes are normalized by its maximal. For details the reader is referred to [9].

new frontiers in Rayleigh-Bénard convection" (33.1 millions of CPU hours on MareNostrum4 in 2018-2019), where DNS simulations of air-filled ($Pr = 0.7$) RBC up to $Ra = 10^{11}$ were carried out using meshes up to 5600M grid points (see dots displayed in Figure 2, top). These results shed light into the flow topology and the small-scale dynamics which are crucial in constructing the turbulent wind and energy budgets [5]. Moreover, it also provided new insights into the preferential alignments of the SGS and its dependence with the Ra-numbers [6], highlighting that the modelization of the SGS heat flux is the main difficulty that (still) precludes reliable LES of buoyancy-driven flows at (very) high Ra-numbers. Shortly, large-eddy simulation (LES) equations arise from applying a spatial commutative filter, with filter length δ, to the incompressible Navier-Stokes and thermal energy equations,

$$\partial_t \overline{\boldsymbol{u}} + (\overline{\boldsymbol{u}} \cdot \nabla)\overline{\boldsymbol{u}} = (Pr/Ra)^{1/2} \ \nabla^2 \overline{\boldsymbol{u}} - \nabla \overline{p} + \overline{\boldsymbol{f}} - \nabla \cdot \tau, \tag{1}$$

$$\partial_t \overline{T} + (\overline{\boldsymbol{u}} \cdot \nabla)\overline{T} = (Ra/Pr)^{-1/2} \nabla^2 \overline{T} \qquad - \nabla \cdot \boldsymbol{q}, \tag{2}$$

where $\overline{\boldsymbol{u}}$, $\overline{T}$ and $\overline{p}$ are respectively the filtered velocity, temperature and pressure, and the incompressibility constraint reads $\nabla \cdot \overline{\boldsymbol{u}} = 0$. The SGS stress tensor, $\tau = \overline{\boldsymbol{u} \otimes \boldsymbol{u}} - \overline{\boldsymbol{u}} \otimes \overline{\boldsymbol{u}}$, and the SGS heat flux vector, $\boldsymbol{q} = \overline{\boldsymbol{u}T} - \overline{\boldsymbol{u}}\,\overline{T}$, represent the effect of the unresolved scales, and they need to be modeled in order to close the system. The most popular approach is the eddy-viscosity assumption, where the SGS stress tensor is assumed to be aligned with the local rate-of-strain tensor, $\mathsf{S} = 1/2(\nabla \overline{\boldsymbol{u}} + \nabla \overline{\boldsymbol{u}}^t)$, *i.e.* $\tau \approx -2\nu_e \mathsf{S}(\overline{\boldsymbol{u}})$. By analogy, the SGS heat flux, $\boldsymbol{q}$, is usually approximated using the gradient-diffusion hypothesis (linear modeling), given by

$$\boldsymbol{q} \approx -\kappa_t \nabla \overline{T} \qquad (\equiv \boldsymbol{q}^{eddy}). \tag{3}$$

Then, the Reynolds analogy assumption is applied to evaluate the eddy-diffusivity, κ_t, via a constant turbulent Prandtl number, Pr_t, *i.e.* $\kappa_t = \nu_e / Pr_t$. These assumptions have been shown to be erroneous to provide accurate predictions of the SGS heat flux [9–11]. Namely, *a priori* analysis showed that the eddy-diffusivity assumption, $\boldsymbol{q}^{eddy}$ (Eq. 3), is completely misaligned

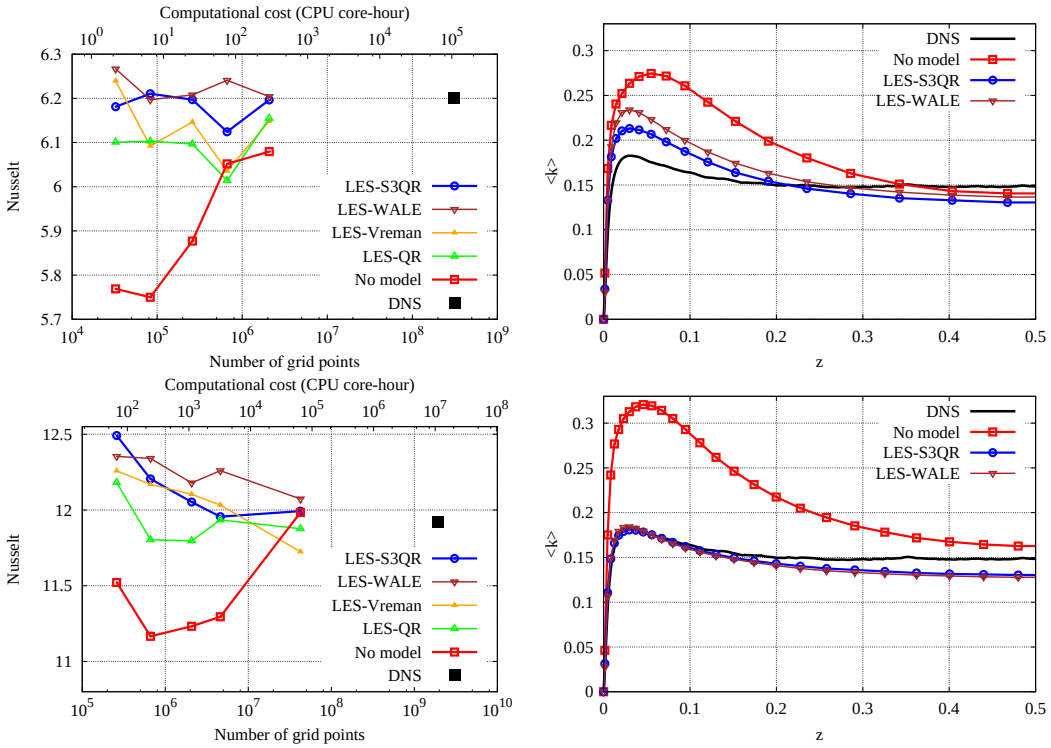

Figure 4: Comparison of LES (and no-model) versus DNS results of liquid-sodium ($Pr = 0.005$) RBC at $Ra = 7.14 \times 10^6$ and 7.14×10^7. Left: average Nusselt for different meshes at $Ra = 7.14 \times 10^6$ (top) and $Ra = 7.14 \times 10^7$ (bottom). Corresponding computational costs at the MareNostrum 4 supercomputer are shown in the top of the plots. Right: LES results of turbulent kinetic energy at cavity mid-width for a $64 \times 36 \times 36$ (top) and $96 \times 52 \times 52$ (bottom) meshes compared with the DNS results obtained with a mesh of $488 \times 488 \times 1280 \approx 305M$.

with the actual subgrid heat flux, $\boldsymbol{q}$ (see Figure 3, left). In contrast, the tensor diffusivity (nonlinear) Leonard model [12], which is obtained by taking the leading term of the Taylor series expansion of $\boldsymbol{q}$,

$$\boldsymbol{q} \approx \frac{\delta^2}{12} \mathsf{G} \nabla \overline{T} \qquad (\equiv \boldsymbol{q}^{nl}), \tag{4}$$

provides a much more accurate *a priori* representation of $\boldsymbol{q}$ (see Figure 3, left). Here, $\mathsf{G} \equiv \nabla \overline{\boldsymbol{u}}$ represents the gradient of the resolved velocity field. It can be argued that the rotational geometries are prevalent in the bulk region over the strain slots, *i.e.* $|\Omega| > |\mathsf{S}|$ (see Refs [4, 9]). Then, the dominant anti-symmetric tensor, $\Omega = 1/2(\mathsf{G} - \mathsf{G}^T)$, rotates the thermal gradient vector, $\nabla \overline{T}$, to be almost perpendicular to $\boldsymbol{q}^{nl}$ (see Eq.4). Hence, the eddy-diffusivity paradigm is only valid in the not-so-frequent strain-dominated areas.

2.2 Nonlinear SGS heat flux models for LES

Since the eddy-diffusivity, $\boldsymbol{q}^{eddy}$, cannot provide an accurate representation of the SGS heat flux, we turn our attention to nonlinear models. As mentioned above, the Leonard model [12] given in Eq.(4) can provide a very accurate *a priori* representation of the SGS heat flux (see

Figure 3, left). However, the local dissipation (in the L2-norm sense) is proportional to $\nabla T \cdot \mathsf{G}\nabla T = \nabla T \cdot \mathsf{S}\nabla T + \nabla T \cdot \Omega \nabla T = \nabla T \cdot \mathsf{S}\nabla T$. Since the velocity field is divergence-free, $\lambda_1^{\mathsf{S}} + \lambda_2^{\mathsf{S}} + \lambda_3^{\mathsf{S}} = \nabla \cdot \boldsymbol{u} = 0$, the eigenvalues of S can be ordered $\lambda_1^{\mathsf{S}} \geqslant \lambda_2^{\mathsf{S}} \geqslant \lambda_3^{\mathsf{S}}$ with $\lambda_1^{\mathsf{S}} \geqslant 0$ (extensive eigendirection) and $\lambda_3^{\mathsf{S}} \leqslant 0$ (compressive eigendirection), and λ_2^{S} is either positive or negative. Hence, the local dissipation introduced by the model can take negative values; therefore, the Leonard model cannot be used as a standalone SGS heat flux model, since it can produce a finite-time blow-up. Attempts to overcome these instability issues are the so-called mixed model [10], where the Leonard model is combined with an eddy-diffusivity model, or the regularization technique proposed in [13] that projects the Leonard model onto a tensor with no energy transfer in case of a negative dissipation event. Similar stability problems are encountered with the nonlinear tensorial model $\boldsymbol{q}^{PD}$ proposed by Peng and Davidson [8],

$$\boldsymbol{q} \approx C_t \delta^2 \mathsf{S}\nabla\overline{T} \qquad (\equiv \boldsymbol{q}^{PD}), \tag{5}$$

$$\boldsymbol{q} \approx -\mathcal{T}_{SGS}\tau\nabla\overline{T} = -\frac{1}{|\mathsf{S}|}\frac{\delta^2}{12}\mathsf{G}\mathsf{G}^T\nabla\overline{T} \qquad (\equiv \boldsymbol{q}^{DH}), \tag{6}$$

whereas the nonlinear model $\boldsymbol{q}^{DH}$ proposed by Daly and Harlow [7] relies on the positive semi-definite tensor $\mathsf{G}\mathsf{G}^T$. Here, $\mathcal{T}_{SGS} = 1/|\mathsf{S}|$ represents the SGS timescale. Notice that the model proposed by Peng and Davidson, $\boldsymbol{q}^{PD}$, can be viewed in the same framework if the SGS stress tensor is estimated by an eddy-viscosity model, *i.e.* $\tau \approx -2\nu_e\mathsf{S}$ and $\mathcal{T}_{SGS} \propto \delta^2/\nu_e$. These two models have shown a much better *a priori* alignment with the actual SGS heat flux, especially the DH model (see Figure 3, middle). Moreover, the DH is numerically stable since the tensor $\mathsf{G}\mathsf{G}^T$ is positive semi-definite. Hence, it seems appropriate to build models based on this tensor. However, the DH model does not have the proper near-wall behavior, *i.e.* $\boldsymbol{q} \propto \langle v'T' \rangle = \mathcal{O}(y^3)$ where y is the distance to the wall. An analysis of the DH model leads to $\mathsf{G}\mathsf{G}^T\nabla\overline{T} = \mathcal{O}(y^1)$ [6]. Therefore, the near-wall cubic behavior is recovered if $\mathcal{T}_{SGS} \propto \mathcal{O}(y^2)$. This is not the case of the timescale used in the Daly and Harlow [7] model, *i.e.* $\mathcal{T}_{SGS} = 1/|\mathsf{S}| = \mathcal{O}(y^0)$. Then, in the quest for more accurate models, we proposed [6] a new family of tensorial SGS heat flux models

$$\boldsymbol{q}^{S2PQ} = -C_{s2pq} P_{\mathsf{G}\mathsf{G}^T}^{-5/2} Q_{\mathsf{G}\mathsf{G}^T} \frac{\delta^2}{12}\mathsf{G}\mathsf{G}^T\nabla\overline{T}, \tag{7}$$

$$\boldsymbol{q}^{S2PR} = -C_{s2pr} P_{\mathsf{G}\mathsf{G}^T}^{-3/2} R_{\mathsf{G}\mathsf{G}^T}^{1/3} \frac{\delta^2}{12}\mathsf{G}\mathsf{G}^T\nabla\overline{T}, \tag{8}$$

$$\boldsymbol{q}^{S2QR} = -C_{s2qr} Q_{\mathsf{G}\mathsf{G}^T}^{3/2} R_{\mathsf{G}\mathsf{G}^T}^{5/6} \frac{\delta^2}{12}\mathsf{G}\mathsf{G}^T\nabla\overline{T}, \tag{9}$$

where $P_{\mathsf{G}\mathsf{G}^T}$, $Q_{\mathsf{G}\mathsf{G}^T}$ and $R_{\mathsf{G}\mathsf{G}^T}$ are the first, second and third invariant of the $\mathsf{G}\mathsf{G}^T$ tensor. This tensor is proportional to the gradient model [14] given by the leading term of the Taylor series expansion of the subgrid stress tensor $\tau(\overline{\boldsymbol{u}}) = (\delta^2/12)\mathsf{G}\mathsf{G}^T + \mathcal{O}(\delta^4)$. Among all the possible candidates, we chose the so-called S2PR model given in Eq.(8) with $C_{s2pr} \approx 12.02$ [6]: it shows a very good representation of the SGS heat flux both in direction and magnitude. Moreover, apart from fulfilling a set of desirable properties (locality, Galilean invariance, numerical stability, proper near-wall behavior, and automatically switch-off for laminar and 2D flows), the proposed model is well-conditioned, and has a low computational cost and no intrinsic limitations for statistically in-homogeneous flows. Testing *a posteriori* this new tensorial SGS heat flux model for air-filled RBC problems at Ra up to 10^{11} is part of our near future research plans.

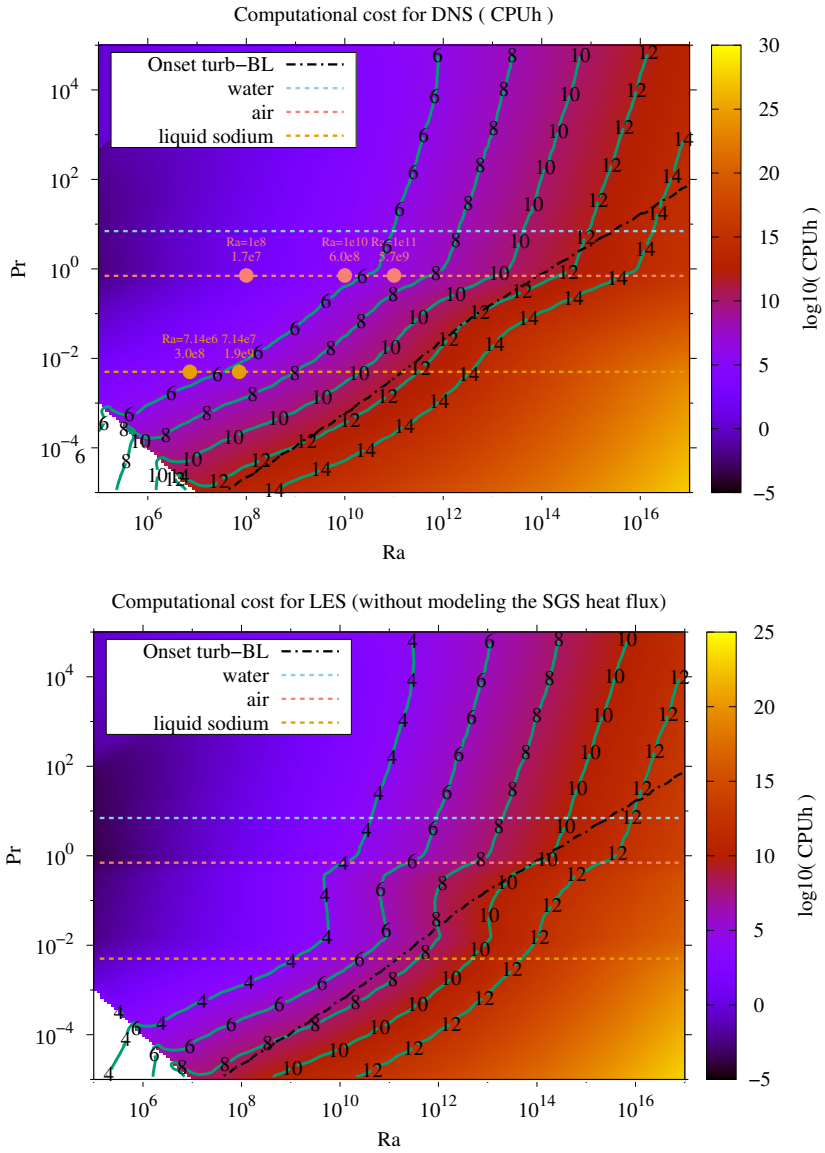

Figure 5: Estimation of the CPU-core hours for DNS (top) and LES (bottom) simulations of RBC in the $\{Ra, Pr\}$ phase space. LES estimations assume that thermal scales are fully resolved, *i.e.* no SGS heat flux model is needed. Green solid isolines represent the $log10$ of the number of CPU-core hours. Three dashed horizontal lines correspond to three different working fluids: water ($Pr = 7$), air ($Pr = 0.7$) and liquid sodium ($Pr = 0.005$). Dots displayed on top of these lines correspond to the DNS simulations carried out in previous studies [4–6]. Black dash-dotted line is an estimation for the onset of turbulence in the thermal boundary layer.

2.3 LES at very low Prandtl numbers

This inherent difficulty can be by-passed by carrying out simulations at low-Prandtl numbers. In this case, the ratio between the Kolmogorov length scale and the Obukhov-Corrsin length

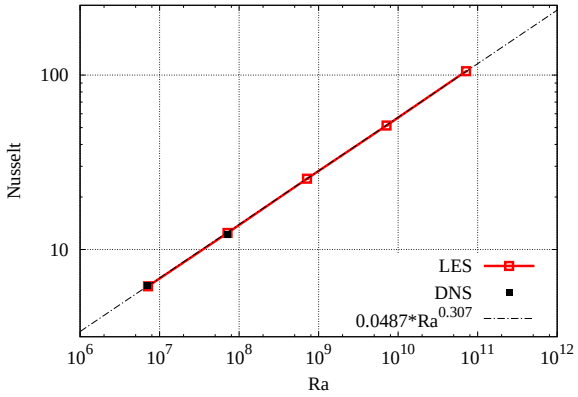

Figure 6: Nusselt versus Rayleigh scaling obtained for a set of LES simulations of RBC at $Pr = 0.005$ (liquid sodium). Configuration details are the same as those used in Ref. [6]. The SGS stress tensor is model with the S3QR eddy-viscosity model [18] whereas no SGS heat flux is needed for this low Pr number. The solid black squares are the DNS results obtained in Ref. [6].

scale (the smallest scale for the temperature field) is given by $Pr^{3/4}$; therefore, for instance, at $Pr = 0.005$ (liquid sodium) we have a separation of more than one decade. Hence, it is possible to combine an LES simulation for the velocity field (momentum equation) with the numerical resolution of all the thermal scales. Results displayed in Figure 4 seem to confirm the adequacy of eddy-viscosity models for this kind of flows. Namely, Figure 4 (left) shows the Nusselt number for a set of meshes and eddy-viscosity models: the WALE model [15], the Vreman model [16], the QR model [17] and the S3QR model [18]. Results obtained without SGS model are also shown to illustrate the effect of the eddy-viscosity models to improve the solution. At first sight it can be observed that, in general, all LES solutions are in rather good agreement with the DNS data even for the coarsest grids ($48 \times 26 \times 26$ for $Ra = 7.14 \times 10^6$ and $96 \times 52 \times 52$ for $Ra = 7.14 \times 10^7$ whereas only the finest ones ($128 \times 72 \times 72$ and $192 \times 104 \times 104$ at $Ra = 7.14 \times 10^6$ and $512 \times 288 \times 288$ at $Ra = 7.14 \times 10^7$) can provide accurate results when the model is switched off. A closer inspection shows that slightly better results are obtained for those eddy-viscosity models (WALE and S3QR) that have the proper near-wall behavior, *i.e.* $\nu_e = \mathcal{O}(y^3)$. To emphasize the benefits of LES modeling, the approximate computational cost of the simulations is displayed in the top horizontal axis of Figure 4 (left): it was measured on the MareNostrum 4 supercomputer and corresponds to a total integration period of 500 time-units. Finally, to see the effect of eddy-viscosity models in more detail, results for the average turbulent kinetic energy are shown in Figure 4 (right) for two meshes and two eddy-viscosity models (WALE and S3QR). All these results seem to confirm the suitability of the eddy-viscosity assumption for buoyancy-driven flows. For more details the reader is referred to [6].

3 CAN WE REACH THE ULTIMATE REGIME?

The results presented in the previous section confirm that low-Pr LES simulations are able to provide accurate predictions of the overall Nu with meshes significantly coarser than for DNS (*e.g.* in practice for $Pr = 0.005$ we can expect mesh reductions in the range 10^2-10^3 for the total

number of grid points). This can be clearly observed in Figure 2 (bottom), where estimations of the mesh size for LES are given with the assumption that thermal scales are fully resolved. This huge gain becomes even more evident in Figure 5 where the number of CPU-core hours (on the basis of MareNostrum 4 supercomputer) is estimated both for DNS and LES. In this case, the difference between DNS and LES goes up to $\mathcal{O}(10^4)$ due to the fact that not only the mesh resolution decreases but also the total number of time-steps. Nowadays, the typical size of a Tier-0 PRACE project is $\mathcal{O}(10^8)$ hours. Therefore, according to the estimations displayed in Figure 5, the so-called ultimate regime of turbulence can be potentially reached carrying out LES at low-Pr using meshes of 10^{10}-10^{11} grid points.

In this regard, Figure 6 shows preliminary LES results at $Pr = 0.005$ (liquid sodium) for Ra-numbers up to $Ra = 7.14 \times 10^{10}$ using a mesh resolution ($768 \times 460 \times 460 \approx 163M$ grid points for the highest Ra) equivalent to those used for the coarsest LES mesh (see Figure 4, top right). Although no evidence of a change of regime is observed (yet), the measured scaling is in very good agreement with the DNS results. Extending these studies to finer grids and higher Ra numbers is part of our near future research plans. Furthermore, these (large-scale) simulations should run efficiently on the variety of modern HPC systems (CPUs, GPUs, ARM,...) while keeping the code easy to port and maintain. In this regard, our *leitmotiv* reads: relying on a minimal set of (algebraic) kernels [19, 20] (*e.g.* sparse-matrix vector product, SpMV; dot product; linear combination of vectors) is crucial for an efficient cross-platform portability.

Acknowledgments. F.X.T. and A.O. are supported by the *Ministerio de Economía y Competitividad*, Spain, RETOtwin project (PDC2021-120970-I00) and by the *Generalitat de Catalunya* RIS3CAT-FEDER, FusionCAT project (001-P-001722). D.S. and J.A.H. are supported by the FI-AGAUR predoctoral grants 2020FI B 00839 and 2022 FI_B1 00204, respectively. Calculations were carried out on MareNostrum 4 supercomputer (projects IM-2022-1-0015 and IM-2022-2-0019) at BSC. The authors thankfully acknowledge these institutions.

References

[1] Siegfried Grossmann and Detlef Lohse. Scaling in thermal convection: a unifying theory. *Journal of Fluid Mechanics*, 407:27–56, 2000.

[2] R. J. A. M. Stevens, E. P. van der Poel, S. Grossmann, and D. Lohse. The unifying theory of scaling in thermal convection: the updated prefactors. *Journal of Fluid Mechanics*, 730:295–308, 2013.

[3] S. Bhattacharya, M. K. Verma, and R. Samtaney. Revisiting Reynolds and Nusselt numbers in turbulent thermal convection. *Physics of Fluids*, 33:015113, 2021.

[4] F. Dabbagh, F. X. Trias, A. Gorobets, and A. Oliva. On the evolution of flow topology in turbulent Rayleigh-Bénard convection. *Physics of Fluids*, 28:115105, 2016.

[5] F. Dabbagh, F. X. Trias, A. Gorobets, and A. Oliva. Flow topology dynamics in a three-dimensional phase space for turbulent Rayleigh-Bénard convection. *Physical Review Fluids*, 5:024603, 2020.

[6] F.X. Trias, F.Dabbagh, A.Gorobets, and C.Oliet. On a proper tensor-diffusivity model for large-eddy simulation of buoyancy-driven turbulence. *Flow, Turbulence and Combustion*, 105:393–414, 2020.

[7] B. J. Daly and F. H. Harlow. Transport equations in turbulence. *Physics of Fluids*, 13:2634, 1970.

[8] S. Peng and L. Davidson. On a subgrid-scale heat flux model for large eddy simulation of turbulent thermal flow. *International Journal of Heat and Mass Transfer*, 45:1393–1405, 2002.

[9] F. Dabbagh, F. X. Trias, A. Gorobets, and A. Oliva. A priori study of subgrid-scale features in turbulent Rayleigh-Bénard convection. *Physics of Fluids*, 29:105103, 2017.

[10] C. W. Higgins, M. B. Parlange, and C. Meneveau. The heat flux and the temperature gradient in the lower atmosphere. *Geophysical Research Letter*, 31:L22105, 2004.

[11] S. G. Chumakov. "*A priori* study of subgrid-scale flux of a passive scalar in isotropic homogeneous turbulence. *Physical Review E*, 78:036313, 2008.

[12] A. Leonard. Large-eddy simulation of chaotic convection and beyond. *AIAA paper*, 97-0304, 1997.

[13] L. Engelmann, M. Klein, and A. M. Kempf. A-posteriori LES assessment of subgrid-scale closures for bounded passive scalars. *Computers & Fluids*, 218:104840, 2021.

[14] R. A. Clark, J. H. Ferziger, and W. C. Reynolds. Evaluation of subgrid-scale models using an accurately simulated turbulent flow. *Journal Fluid Mechanics*, 91:1–16, 1979.

[15] F. Nicoud and F. Ducros. Subgrid-scale stress modelling based on the square of the velocity gradient tensor. *Flow, Turbulence and Combustion*, 62(3):183–200, 1999.

[16] A. W. Vreman. An eddy-viscosity subgrid-scale model for turbulent shear flow: Algebraic theory and applications. *Physics of Fluids*, 16(10):3670–3681, 2004.

[17] R. Verstappen. When does eddy viscosity damp subfilter scales sufficiently? *Journal of Scientific Computing*, 49(1):94–110, 2011.

[18] F. X. Trias, D. Folch, A. Gorobets, and A. Oliva. Building proper invariants for eddy-viscosity subgrid-scale models. *Physics of Fluids*, 27(6):065103, 2015.

[19] X. Álvarez, A. Gorobets, F. X. Trias, R. Borrell, and G. Oyarzun. HPC^2 - a fully portable algebra-dominant framework for heterogeneous computing. Application to CFD. *Computers & Fluids*, 173:285–292, 2018.

[20] X. Álvarez, A. Gorobets, and F. X. Trias. A hierarchical parallel implementation for heterogeneous computing. Application to algebra-based CFD simulations on hybrid supercomputers. *Computers & Fluids*, 214:104768, 2021.